1222
doi:10.1017/S1431927622005098
Microsc. Microanal. 28 (Suppl 1), 2022

Montage Cryo-Electron Tomography: a High Throughput and Flexible Data Collection Scheme to Explore In-situ Cellular Landscapes while Preserving High-Resolution Data

Jae Yang[1,2,3], Matt Larson[1,2,3], Bryan Sibert[1,2,3], Elizabeth Wright[1,2,3,4*]

1. Department of Biochemistry, University of Wisconsin, Madison, WI, USA
2. Cryo-Electron Microscopy Research Center, Department of Biochemistry, University of Wisconsin, Madison, WI, USA
3. Midwest Center for Cryo-Electron Tomography, Department of Biochemistry, University of Wisconsin, Madison, WI, USA
4. Morgridge Institute for Research, Madison, WI, USA
* Corresponding author: erwright2@wisc.edu

Cryo-electron tomography (cryo-ET) is a powerful tool for visualizing complex biological systems in-situ and in 3D [1]. In cryo-ET, a series of images are acquired while the specimen is incrementally tilted, the information is combined computationally to reconstruct a 3D tomogram [2]. Sub-tomogram averaging (STA) can then be applied to sub-classes of particles in a tomogram. The particles are averaged to produce higher signal-to-noise and higher resolution structures [3]. Currently, the highest resolution STA are sub 4 Å [4], however, this is a-typical and most STA are in the 10 to 25 Å range [1]. The pursuit of high-resolution STA generally constrains the field of view within one tomogram because of pixel size and sampling requirements [5]. Biological samples under cryo-conditions are extremely dose intolerant [1] and this restricts both the applicable total dose and possibility of sampling the same object more than once at different magnifications for tilt series collection. To overcome some of the challenges associated with cryo-ET of biological specimens, we demonstrate our adaption of montage tilt series collection [6] for cryogenically preserved samples.

Briefly, we implemented a beam/image-shift montage acquisition scheme to acquire overlapping tiles of regular arrays (Figure 1A, B) at each tilt angle. We considered the beam size relative to the camera frame and illuminated area, and to account for the impact of Fresnel fringes [7], and options for automated stitching [8]. At a constant magnification (pixel size 1.5 to 7 Å) and defocus (- 5 μm) typical for cryo-ET, linear relationships were observed between illuminated areas on a triple-condenser lens Titan Krios system (non-fringe-free regular system), the beam projected on the camera plane, and the associated fringeless illuminate area. We benchmarked montage cryo-ET at the magnification of 4.6 Å per pixel (EFTEM, 20 eV GIF) and found that an optimal overlap of 15 to 20% in the fringe-impacted x-axis and 10% in fringe-less y-axis on a regular 5k x 4k rectangle K3 camera achieves consistently automated seamless stitching. Regular 3x3 or 3x4 cryo-ET montages produce 6.8 x 5.3 μm or 7.8 x 6.5 μm fields of view (FOV), respectively, compared to a single view of 2.6 x 1.8 μm (4.6 Å per pixel). Increases in TEM magnification also increases the impact of Frensnel fringes on individual image tiles, leading to stitching artifacts along overlapping tile zones even when an enlarged illuminated area was adopted for compensation (Figure 1A). To spread the uneven accumulation of dose over the overlapping zones, we further employed an additional global translational shift of up to 0.8 μm extending from the central tile of a montage pattern (Figure 1B), as suggested by simulation results from TomoGrapher (Figure 1C, https://github.com/wright-cemrc-projects/cryoet-montage), an open-source simulation tool we developed to visualize and optimize tilt series collection routines and dose accumulation. Via a

regular 3x3 montage cryo-ET, we were able to capture an extended FOV of a thin cryo-FIB milled lamella of a vitrified A549 cell [9] (Figure 1D).

To maximize the throughput, we explored the application of individual tile tilt series and independently reconstructing them into tile tomograms. We compared the defocus, CTF estimation, and Fourier space information of the stitched montage tilt series and individual tile tilt series at different tiling locations. Correlation with TomoGrapher simulations, we determined the impact of translation, dose, and overlap stitching on preserving high-resolution information for STA of the respiratory syncytial virus (RSV) F glycoprotein. As shown in Figure 2, we observed RSV F pairs oriented in an anti-parallel symmetrical conformation, relative to the M matrix underneath, as reported in previous data sets collected via regular tilt series schemes [10].

In summary, we demonstrate that montage cryo-ET is a robust workflow suited for capturing both comprehensive fields of view and preservation of high-resolution structural information for downstream STA. By using regular array montage image-shift cryo-ET, the overall data collection throughput was increased and post-processing workflows were flexible and supported both segmentation and STA [11].

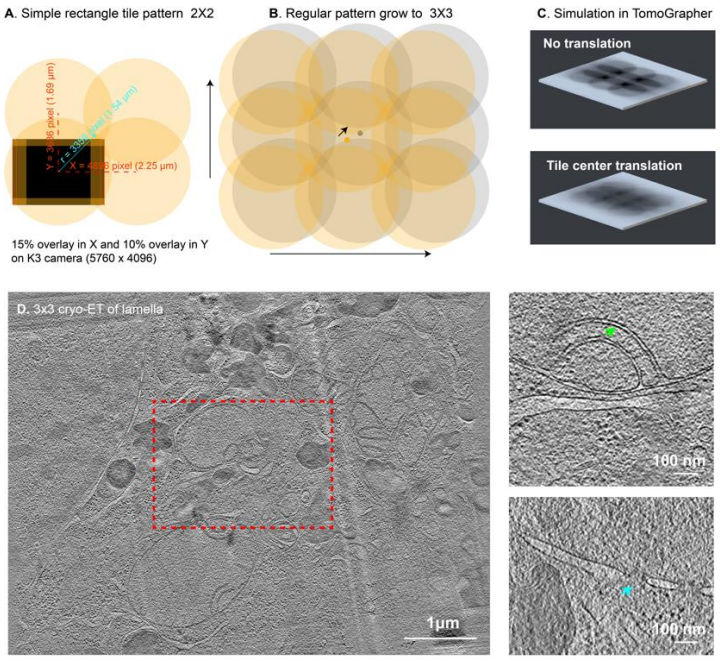

Figure 1. Extended field of view of cryogenic lamella of a mammalian cell via montage cryo-ET. (A-B) Montage cryo-ET collection scheme coupled to simulations in (C) TomoGrapher. (D). Left: 3x3 montage cryo-ET of lamella show 6.8 x 5.3 µm landscape versus a single regular tilt series (red boxed) of 2.6 x 1.8 µm at 4.6 Å per pixel; Right: enlarged views to show ultrastructural details of mitochondria ATPase (green arrow) and nuclear pore complex (blue arrow).

https://doi.org/10.1017/S1431927622005098 Published online by Cambridge University Press

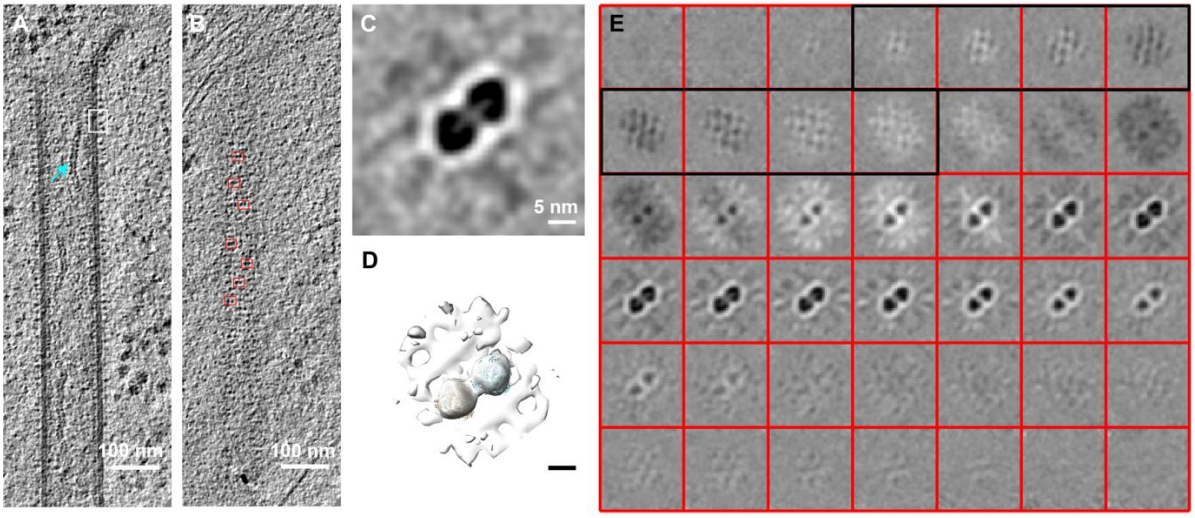

Figure 2. Individual tile tomograms from 3x3 montage cryo-ET collection of RSV filaments. (A-B) Different z-slices of tile tomograms reveal structural information of ribonucleoprotein (cyan arrow) and RSV F glycoprotein pairs at 4.6 Å per pixel. (C-E) Sub-tomogram averages of RSV F pairs (n = 2250) slicing through from the bottom to the top (E) showing the M matrix underneath (black boxed views in E). Isosurface renderings of the F pair in (C) with F pre-fusion trimer models (PDB: 5w23). The volume was low pass filtered to 35 Å.

References.

[1] FKM Schur, Current Opinion in Structural Biology **58** (2019), p. 1.
[2] DN Mastronarde and SR Held, Journal of Structural Biology **197**(2) (2017), p. 102.
[3] A von Appen et al., Nature, **526**(7571) (2015), p. 140.
[4] FK Schur et al., Science, **353**(6298) (2016), p. 506.
[5] CE Shannon, Proceedings of the IRE **37**(1) (1949), p. 10.
[6] DN Mastronarde et al., Microscopy and Microanalysis **14**(S2) (2008), p. 106.
[7] K Fukushima, H Kawakatsu and A Fukami, Journal of Physics D: Applied Physics **7**(2) (1974), p. 257.
[8] R Chen et al., Procedia Comput Sci **20** (2014), p. 2295.
[9] A Rigort et al., Journal of Structural Biology **172**(2) (2010), p. 169.
[10] BS Sibert et al., bioRxiv (2021), p. 2021.10.13.464285.
[11] This work was supported in part by the University of Wisconsin, Madison, the Department of Biochemistry at the University of Wisconsin, Madison, and public health service grants R01 GM114561 and U24 GM139168 to E.R.W. from the NIH. We are grateful for the use of facilities and instrumentation at the Cryo-EM Research Center in the Department of Biochemistry at the University of Wisconsin, Madison.